YMTHE, Volume *27*

Supplemental Information

Weak Agonistic LPS Restores Intestinal Immune Homeostasis

Alex Steimle, Lena Michaelis, Flaviana Di Lorenzo, Thorsten Kliem, Tobias Münzner, Jan Kevin Maerz, Andrea Schäfer, Anna Lange, Raphael Parusel, Kerstin Gronbach, Kerstin Fuchs, Alba Silipo, Hasan Halit Öz, Bernd J. Pichler, Ingo B. Autenrieth, Antonio Molinaro, and Julia-Stefanie Frick

Supplemental information

Supplemental information 1:

Comparison of surface molecule expression pattern of colonic lamina propria (cLP) CD11c+ cells and bone-marrow derived dendritic cells (BMDCs)

To verify the similarity of *ex vivo* isolated cLP CD11c+ cells with *in vitro* generated BMDCs in terms of expression of important surface markers, we stained both cell types with fluorophore-coupled antibodies for detection of CD11c, Ly6G, Ly6G, CD64, CD45R, CD45, CD103, CD11b and MHC-II (Figure S1). Viable cLP $CD11c^{+}$ single cells and viable BMDC single cells were demonstrated to provide similar expression of surface total MHC-II, CD45 and non-expression of Ly6G, Ly6C, CD64 and CD45R. We could detect slight differences in the expression of $CD103^{pos/neg}CD11b^{pos/neg}$ dendritic cell subpopulations, with BMDCs providing a slightly higher proportion of $CD103^{neg}CD11b^{pos}$ $CD11c^{+}$ cells while the $CD103^{neg}CD11b^{neg}$ subpopulation is slightly more frequent among cLP CD11c+ cells. However, these minor differences are assumed to be irrelevant for the performed experiments and conclusions.

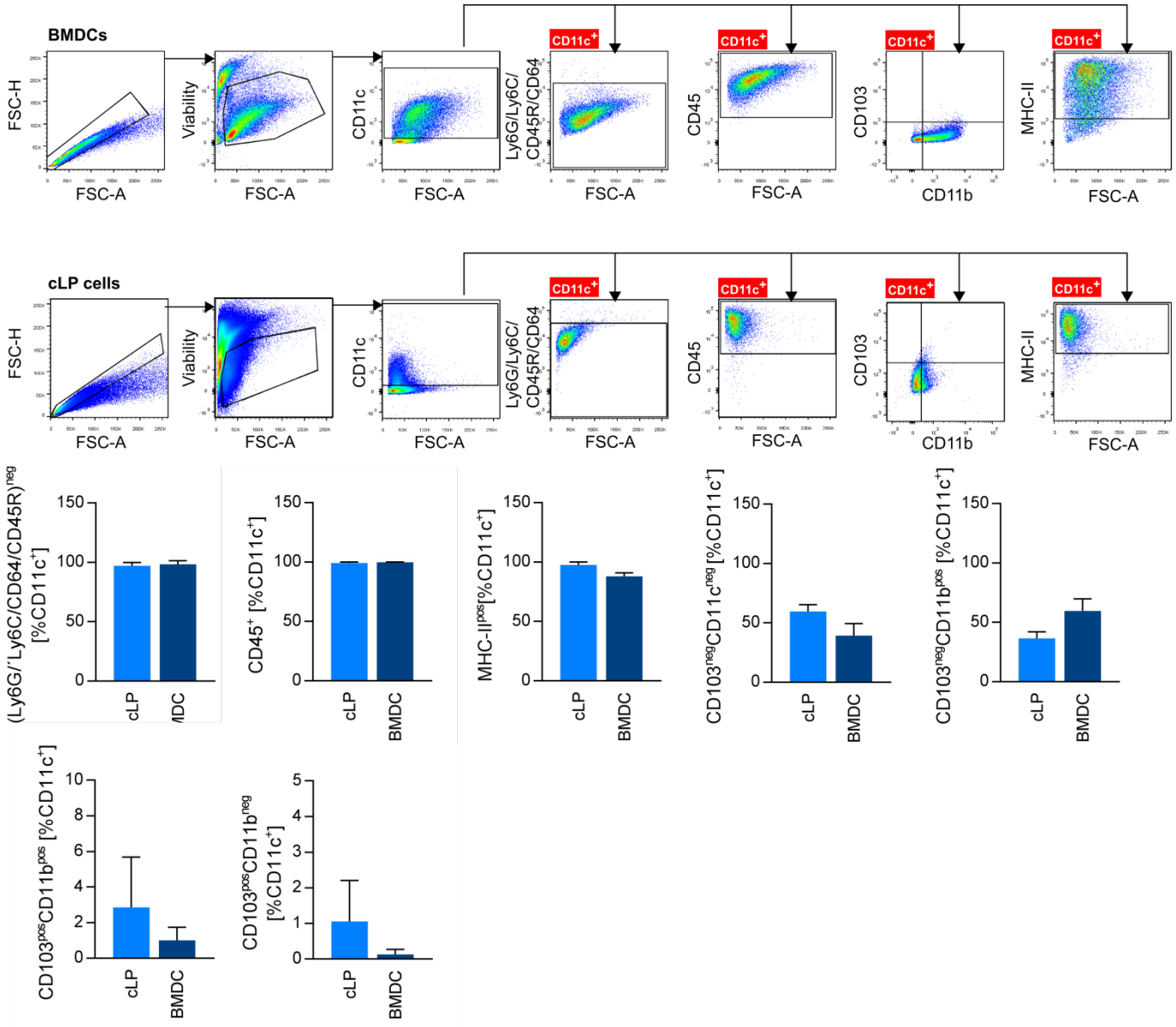

Figure S1: **Comparison between BMDCs and cLP CD11c+ cells.**

Bone-marrow derived dendritic cells (BMDCs) were generated as described in the Materials and Methods section. Colonic lamina propria (cLP) cells were isolated from $Rag1^{-/-}$ mice as described in the Materials and Methods section. Both cell types were stained with a fixable viability dye as well as with antibodies detecting CD11c, Ly6G, Ly6G, CD64, CD45R, CD45, CD103, CD11b and MHC-II. Upper panel and middle panel: Gating strategy for BMDCs (upper panel) and cLP cells (middle panel). Single cells

(FSC-A vs. FSC-H) were gated for viable cells. Viable single cells were gated for CD11c expression and $CD11c^+$ cells were analyzed for expression of Ly6G, Ly6C, CD64, CD45R, CD103, CD11b and MHC-II. Lower panel: Determination of surface expression of the respective surface molecules as a proportion of all $CD11c^+$ cells (n = 15 for each cell type). Columns and error bars represent mean ± SD

<u>Supplemental information 2</u>:

Gating strategy to determine CD40 surface expression as well as to define the subpopulation of MHC-II high positive cells

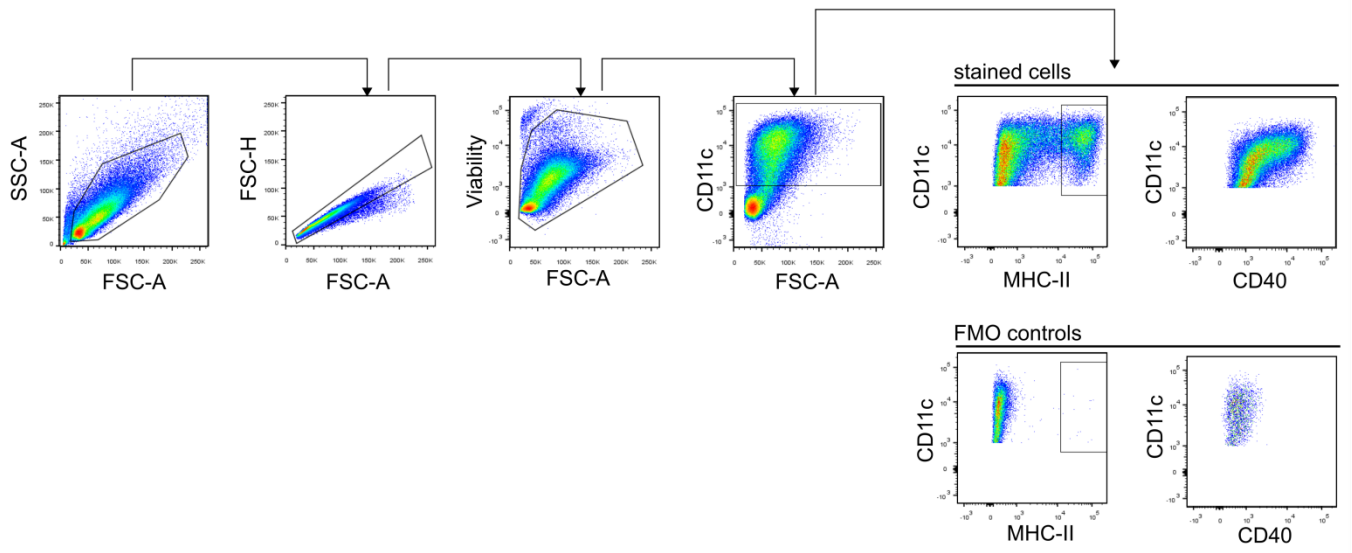

Figure S2: **BMDC gating strategy**

Gating strategy to determine CD40 surface expression as well as to define the subpopulation of MHC-II high positive cells. Viable, single $CD11c^{+}$ cells were stained for MHC-II and CD40 surface expression. Analysis of MHC-II surface expression was assessed by determination of the MHC-II high positive population, which is increased during DC maturation. CD40 expression was determined by measuring Median Fluorescence Intensity (MFI). The upper panel shows stained cells while the lower panel shows fluorescence-minus-one controls to determine $MHC\text{-}II^{neg}$ and $CD40^{neg}$ cells.

Supplemental information 3:

Heat-killed *Bacteroides* strains induce the same semi-mature phenotype in BMDCs as viable *Bacteroides* strains.

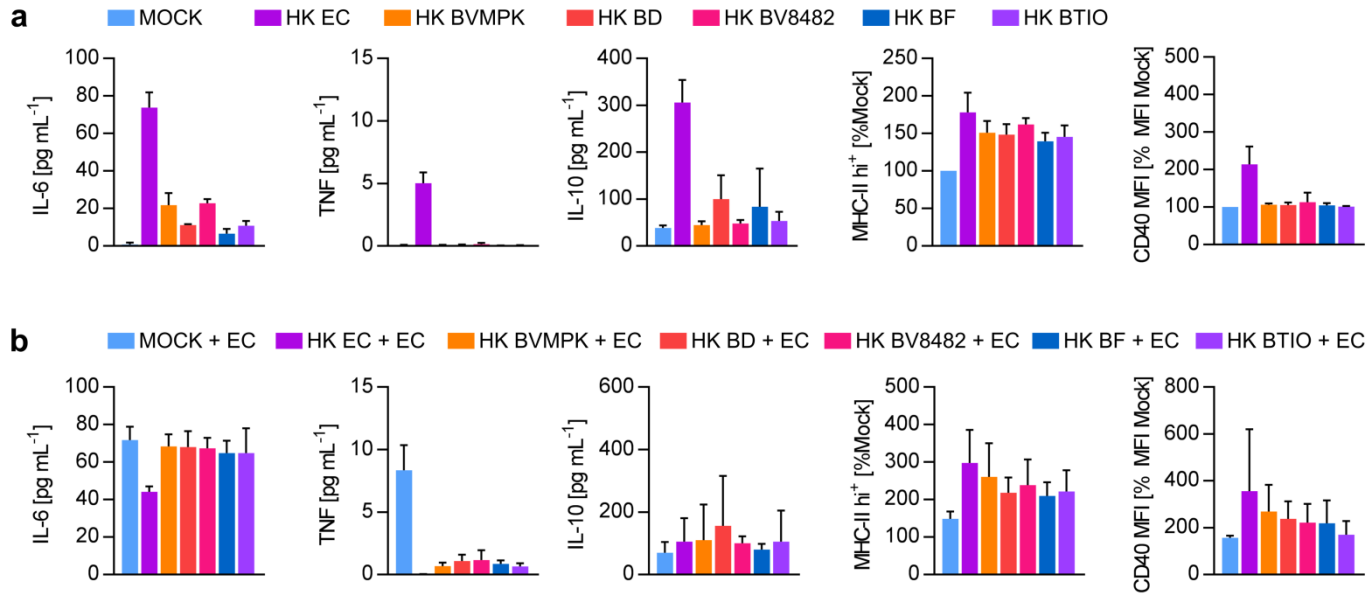

Figure S3: Heat-killed *Bacteroides* species induce the same hyporesponsive phenotype in CD11c+ cells as viable *Bacteroides* species

a) Stimulation of CD11c+ bone-marrow derived dendritic cells (BMDCs) generated from wt C57BL/6 mice (n=3) with PBS (Mock), heat-killed *E. coli* mpk (HK EC),heat-killed *B. vulgatus mpk* (HK BVMPK), heat-killed *B. dorei* (HK BD), heat-killed *B. vulgatus* ATCC8482 (HK BV8482), heat-killed *B. fragilis* (HK BF) and heat-killed *B. thetaiotaomicron* (HK BTIO) for 16 h at MOI 1. Cytokine secretion was detected by ELISA. Surface expression of MHC-II and CD40 was detected by flow cytometry and the population of MHC-II hi+ cells and CD40 MFI, respectively, was normalized to the mock control of BMDCs generated from the same individual. Columns and error bars represent mean ± SD.

b) *wt* BMDCs were stimulated with PBS (mock), HK EC, HK BVMPK, HK BD, HK BV482, HK BF and HK BTIO at MOI 1 for 24h (prime). Cell culture medium removed and exchanged for fresh medium before stimulation (challenge) with viable EC for additional 16 h. Cytokine secretion was detected by ELISA. Surface expression of MHC-II and CD40 was detected by flow cytometry and the population of MHC-II hi+ cells and CD40 MFI, respectively, was normalized to the mock-primed and EC-challenged control of BMDCs generated from the same individual. Columns and error bars represent mean ± SD.

Supplemental information 4:

Evaluation of TAK252 as a specific TLR4 inhibitor

To verify that TAK242 selectively inhibits TLR4 signalling, we treated BMDCs generated from wildtype mice with 10 µM TAK242 1h prior stimulation for 16 h with PBS (mock) LPS-EK as potent TLR4 ligand, FLA-ST as potent TLR5 ligand and PAM2CSK4 a potent TLR2 ligand, all at a final concentration of 100 ng/mL. Secretion of IL-6 as an indicator of TLR signalling was detected by ELISA. TAK242 significantly inhibited IL-6 secretion in cells stimulated with LPS-EK but showed no significant inhibitory activity in cells stimulated with FLA-ST or PAM2CSK4. This result supports findings by Lii *et al*., Takashima *et al.* and Matsunaga *et al* [1-3], observing no or only marginal binding of TAK242 to other TLRs compared to TLR4. We therefore consider TAK242 as a selective TLR4 inhibitor.

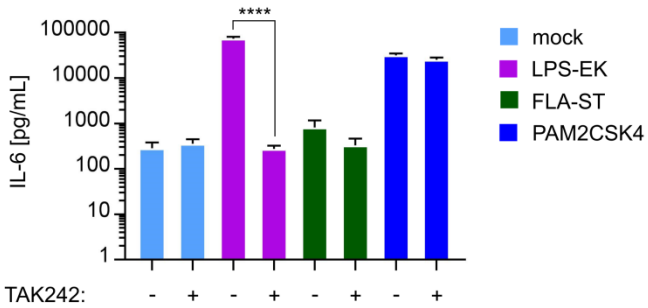

Figure S4:

TAK242 selectively inhibits TLR4 signaling

The competitive TLR4 antagonist TAK242 was added to CD11c+ bone-marrow derived dendritic cells (BMDCs) generated from wt C57BL/6 mice at a final concentration of 10 µM 1h prior to a stimulation for 16 h with with PBS (Mock) or ligands for TLR4 (LPS-EK, Invivogen), TLR5 (FLA-ST, Invivogen) and TLR2 (PAM2CSK4, Invivogen), all at a final concentration of 100 ng/mL. IL-6 secretion was detected by ELISA. Inhibitory activity of TAK242 is indicated by a significant reduction of IL-6 secretion in LPS stimulated cells but not in FLA-ST or PAM2CSK4-stimulated cells upon TAK242 treatment compared with mere TLR ligand stimulation. Columns and error bars represent mean ± SD.

Supplemental information 5:

Gating strategy to determine intracellular ALDH activity

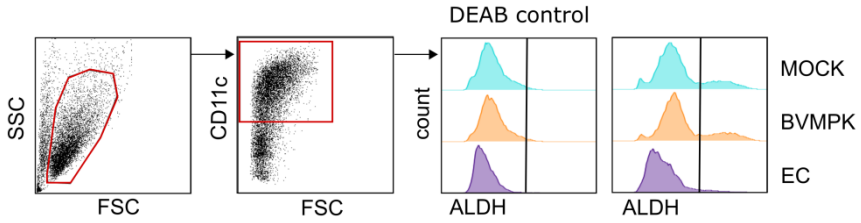

Figure S5: ALDH activity assay

Stimulation of $CD11c^+$ BMDCs generated from wt C57BL/6 mice with PBS (mock), *B. vulgatus* mpk (BVMPK) and *E. coli* mpk (EC) for 16 h. ALDH activity in stimulated cells was then analysed with the Aldefluor kit (Stemcell). Flow cytometric analysis with additional staining for CD11c was used to determine the mean fluorescence intensity (MFI) of $CD11c^+$ $ALDH^+$ cells. DEAB treated samples (left histogram panel) were used for determination of background fluorescence and defining $ALDH^+$cells , indicated by exemplary samples shown in right histogram panel.

Supplemental information 6:

LPSBV-induced semi-maturation of BMDCs requires TLR4, but not TLR2-signaling

We stimulated BMDCs generated from wildtype, TLR2-deficient, TLR4-deficient and TLR2xTLR4-double deficient mice with PBS (negative control), LPSBV (100 ng/mL) and EC (MOI1, positive control) and checked for subsequent secretion of pro-inflammatory cytokines IL-6 and TNF as well as surface expression of MHC-II and CD40. As already demonstrated in the main manuscript, stimulation of wildtype BMDCs with LPSBV resulted in intermediate secretion of IL-6, low to intermediate expression of MHC-II and CD40 as well as to absence of TNF compared to the EC positive control. IL-6 and TNF expression as well as increase in surface expression of MHC-II and CD40 was completely abolished using TLR4-deficient and TLR2xTLR4-double deficient BMDCs. Importantly, stimulation of TLR2-deficient BMDCs with LPSBV resulted in the same expression pattern of the detected cytokines and surface markers as LPSBV stimulation of wildtype BMDCs. To assess the contribution of a potential TLR2-signaling to the induction of LPSBV-induced semi-maturation in BMDCs, we primed TLR2-deficient BMDCs with PBS, LPSBV and EC and challenged them with either PBS or EC as a second stimulus as already demonstrated for wildtype BMDCs (Fig. 3). As shown in Figure S6b, hyporesponsiveness in terms of TNF and MHC-II expression was induced by LPSBV-priming, indicating that TLR2-mediated signaling is dispensable for LPSBV-induced BMDCs semi-maturation. Taken together, these results indicate that (1) either LPSBV or a potential contaminant induce a slight activation of TLR2-mediated signaling in mTLR2-HEK cells, (2) TLR4-signaling is far more important than TLR2-signaling for LPSBV-mediated effects on BMDCs in terms of cytokine expression and MHC-II/CD40 surface expression in response to stimulation with LPSBV preparations, (3) LPSBV or a potential contaminant does not activate TLR2 signaling in BMDCs and (4) LPSBV-induced MD-2/TLR4 receptor-signaling is essential for induction of semi-maturation in BMDCs.

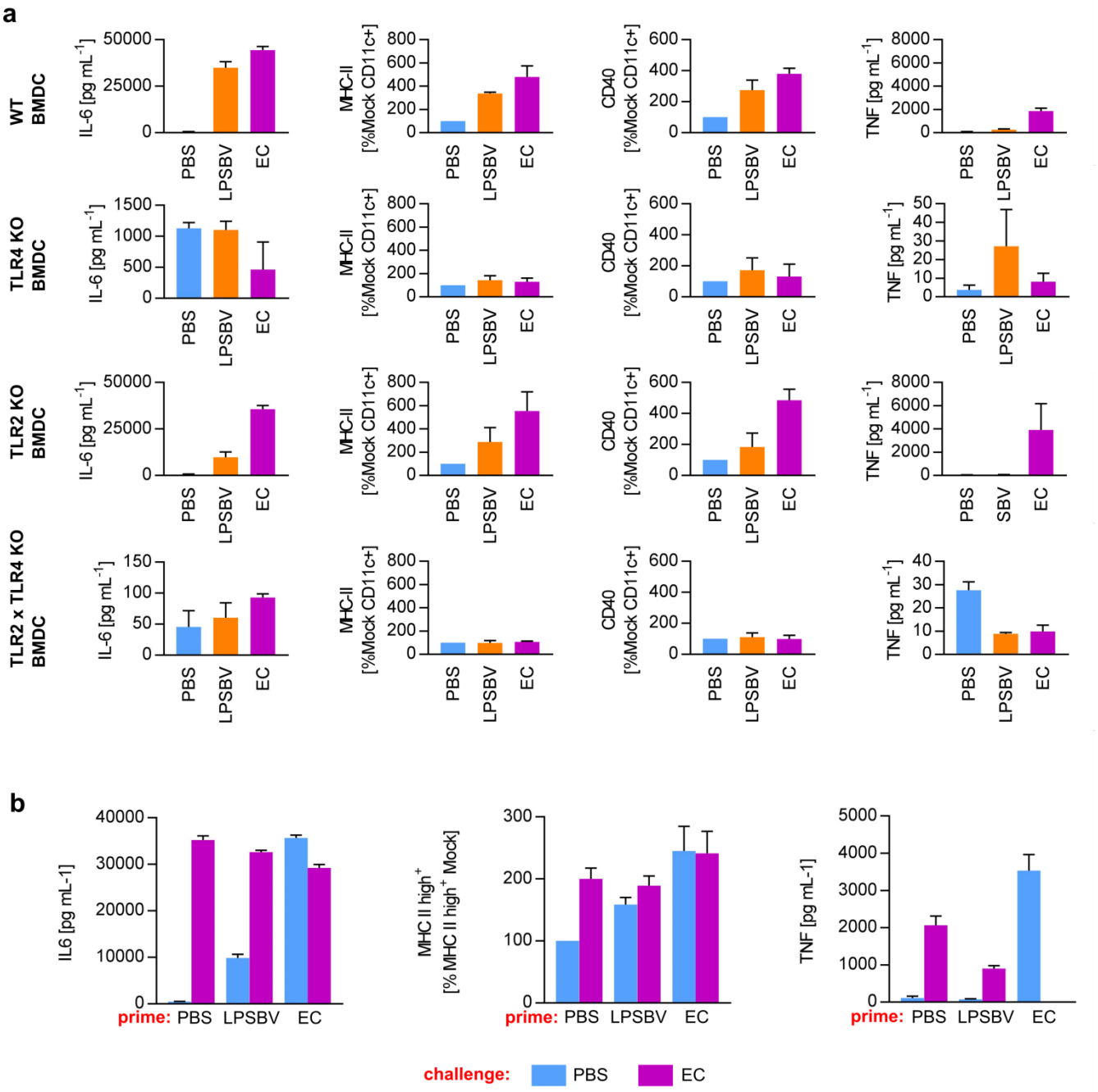

Figure S6: LPSBV-induced semi-maturation of BMDCs requires TLR4, but not TLR2-signaling

a) Stimulation of CD11c+ bone-marrow derived dendritic cells (BMDCs) generated from wt C57BL/6, TLR2-deficient, TLR4-deficient and TLR2xTLR4 double-deficient mice (n=4-8) with PBS (Mock), *E. coli* mpk (EC) and *B. vulgatus* mpk LPS (LPSBV). Cytokine secretion was detected by ELISA. Surface expression of MHC-II and CD40 was detected by flow cytometry and the population of MHC-II hi+ cells and CD40 MFI, respectively, was normalized to the mock control of BMDCs generated from the same individual. Columns and error bars represent mean ± SD.

b) TLR2-deficient BMDCs were stimulated with PBS (mock), EC or LPSBV for 24h (prime). Cell culture medium was removed and exchanged for fresh medium before stimulation (challenge) with EC or PBS for additional 16 h. Cytokine secretion was detected by ELISA. Surface expression of MHC-II and CD40 was detected by flow cytometry and the population of MHC-II hi+ cells and CD40 MFI, respectively, was normalized to the PBS-primed and PBS-challenged control of BMDCs generated from the same individual. Columns and error bars represent mean ± SD.

Supplemental information 7:

Biotinylation of LPSBV does not affect weak agonistic properties of LPSBV

To verify that biotinylation of LPSBV does not affect the weak agonistic properties of LPSBV, HEK cells overexpressing the mouse CD14/MD-2/TLR4-receptor complex were stimulated with LPSBV, bioLPSBV and LPSEC. We determined resulting expression of IL-8 as a measure of NFκB activation. We did not detect any differences in the NFκB activation in response to LPSBV compared to bioLPSBV (Figure 7)

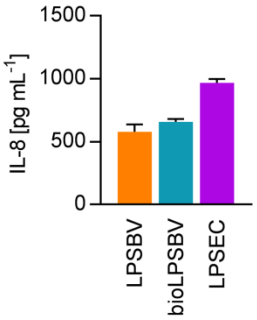

Figure S7: **Influence of LPSBV biotinylation on TLR4 receptor activation.**

mTLR4-HEK cells were stimulated with 10 ng/mL LPSBV, biotinylated LPSBV (bioLPSBV) and LPSEC. Resulting IL-8 concentration as a measure of intracellular NFκB activation was detected by ELISA. Columns and error bars represent mean ± SD.

Supplemental information 8:

Determination of quasi dissociation constants K_D of LPSBV and LPSEC

The observation that both LPS structures, LPS_{BV} and LPS_{EC}, showed different immunological effects on DCs *in vitro*, prompted us to define their binding affinity to the MD-2/TLR4 receptor complex. We established an experimental setting to determine *quasi* dissociation constants (K_D) of both LPS structures using biotinylated LPS_{BV} ($bioLPS_{BV}$). We are aware of the fact that we cannot determine real K_D-values since we do not know the exact molarity of the used LPS solutions. The assembly of amphiphilic LPS monomers into micelles, vesicles or even more complicated structures is highly dependent on the surrounding buffer and salt conditions and is therefore hardly predictable. This exacerbated the determination of the molarity of LPS monomers which effectively have access to the receptor, rendering them "active ligands" thus contributing to K_D values. However, assuming that (1) $bioLPS_{BV}$ and LPS_{EC} provide a comparable monomeric molecular weight, (2) $bioLPS_{BV}$ and LPS_{EC} behave in a similar chemical manner under the experimental conditions and (3) all experiments were carried out incubating both LPS at the same time, we can speculate that a qualitative comparison using K_D-values in the unit [g L^{-1}] instead of [mol L^{-1}] is qualifiable for a comparison of their binding affinity. In order to determine K_D values for both LPS structures, we used human embryonic kidney (HEK) cells which were stably transfected with a plasmid encoding for murine CD14, MD-2 and TLR4 (HEK-mTLR4). These latter were expressed by HEk-mTLR4 cells in excess and in equal amount by HEK-mTLR4 cells in all executed experiments, representing a fundamental prerequisite for K_D determination. LPS_{BV} was biotinylated ($bioLPS_{BV}$) as described in the experimental sections and its immunological behaviour was tested and compared to non-biotinylated LPS_{BV}. Since we could not detect any differences in the immunological behaviour (data not shown), we concluded that biotinylation did not affect the interaction with the receptor complex. We incubated HEK-mTLR4 cells with various concentrations of $bioLPS_{BV}$ and we then visualized bound $bioLPS_{BV}$ by adding PE-coupled streptavidin followed by flow cytometric analysis of the resulting PE fluorescence. As shown in Fig. S6a, non-biotinylated LPS and cells without addition of any LPS did not contribute to the PE fluorescence signal. The resulting PE-fluorescence in $bioLPS_{BV}$-treated samples was dependent on $bioLPS_{BV}$ concentration and showed a classical perpendicular hyperbola binding curve of a ligand to its respective receptor (Fig. S8a, right panel). In order to determine K_D of $bioLPS_{BV}$ and LPS_{EC} we simultaneously incubated HEK-mTLR4 cells with different concentrations of both LPS for 1 h and detected resulting PE fluorescence, which is directly proportional to the amount of bound $bioLPS_{BV}$ (Fig. S8b). In order to define the K_D value of $bioLPS_{BV}$, various concentrations of this LPS alone without addition of LPS_{EC} were used. The K_D equalled the concentration of $bioLPS_{BV}$ corresponding to the half maximal MFI PE intensity, which could be determined as 0.412 mg L^{-1}. In other words, adding 0.412 mg L^{-1} to the used 1 x 10^5 HEK-mTLR4 cells led to occupation of half of the available MD-2/TLR4 binding sites (Fig. S8c). In order to determine K_D of LPS_{EC}, several concentrations of LPS_{EC} were co-incubated with different concentrations of $bioLPS_{BV}$, resulting in 4 different binding curves representing the 4 employed LPS_{EC} concentrations (Fig. S8d). The resulting binding curves follow the equation

$$(1)\ MFI\ PE = \frac{n[bioLPS_{BV}]}{[bioLPS_{BV}] + K_D(bioLPS_{BV}) \times \left(1 + \frac{[LPS_{EC}]}{K_D(LPS_{EC})}\right)}$$

with n being the number of different binding sites (which was assumed to be 1 in our case). The binding curves shown in Fig. S8d were then plotted into a double reciprocal form resulting in 4 different straight lines whose slopes were determined using GraphPad Prism (Fig. S8e). The slopes obtained from Figure S8e were afterwards plotted against the respective LPS_{EC} concentration resulting in a straight line whose intersection with the x-axis represented the negative value of the LPS_{EC} binding constant which was determined to be 0.304 mg L^{-1}, being in the same biologically relevant range as $bioLPS_{BV}$ K_D. Therefore, based on the above described experiments, we can conclude that LPS_{BV} and LPS_{EC} provide similar binding affinity to the MD-2/TLR4 receptor complex.

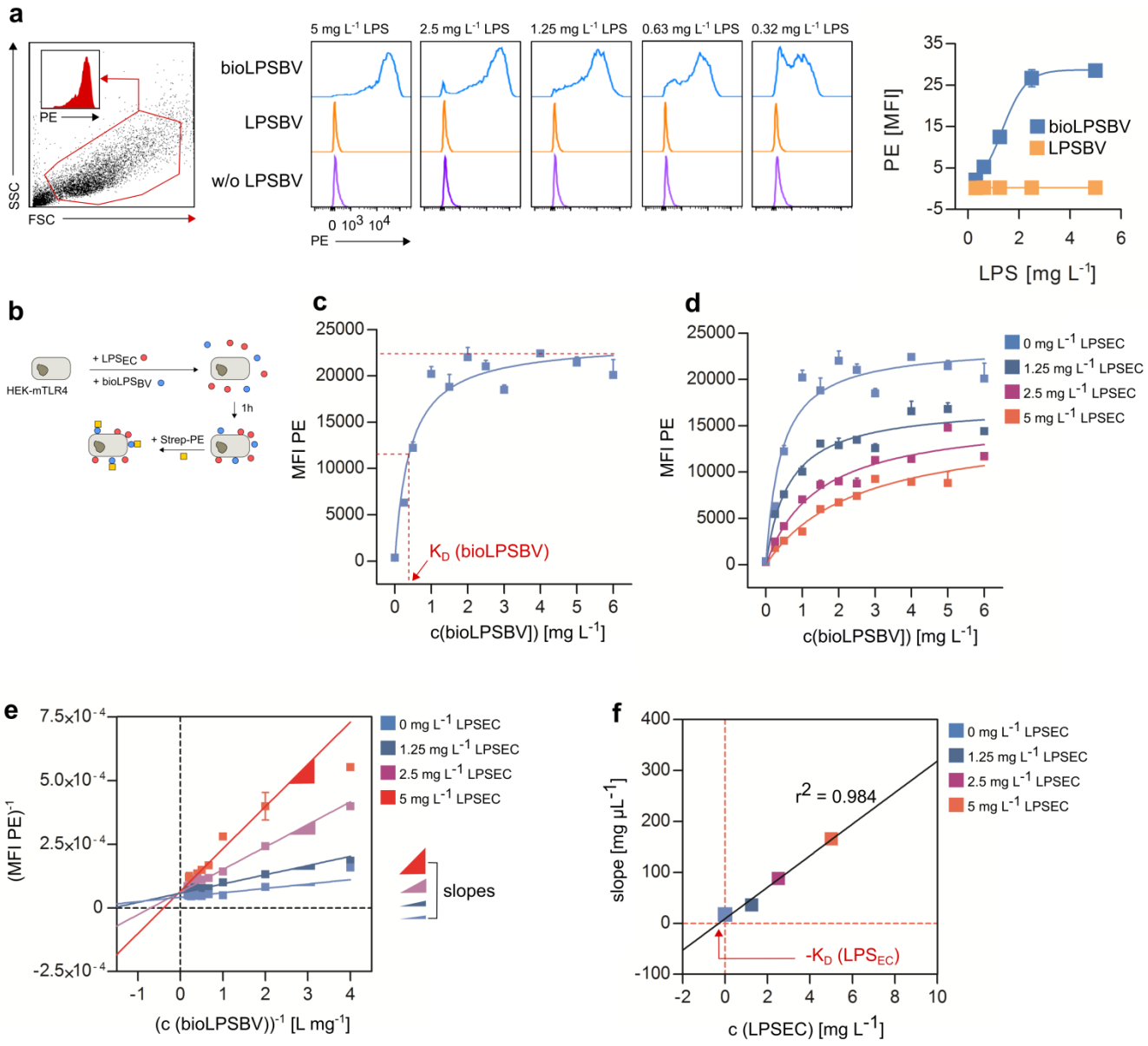

Figure S8: *B. vulgatus* mpk LPS and *E. coli* mpk LPS provide similar binding affinity to the MD-2/TLR4 receptor complex.

(a) Human embryonic kidney (HEK) cells expressing murine CD14, MD-2 and TLR4 (HEK-mTLR4) were co-incubated with *B. vulgatus* mpk LPS (LPSBV), biotinylated *B. vulgatus* mpk LPS (bioLPSBV) or PBS (w/o LPS_{BV}) at several concentrations. PE-coupled streptavidin (Strep-PE) was added to each sample in constant concentrations. Cells were washed and analysed afterwards for PE fluorescence using flow cytometry. Left panel: gating strategy to determine intact HEK-mTLR4 cells. Middle panel: representative histograms of PE fluorescence of intact HEK-mTLR4 cells that were treated as described above. Right panel: Detected mean PE fluorescence intensity (PE (MFI)) as a function of used $bioLPS_{BV}$ concentration.

(b) experimental setting for the determination of LPS binding affinity: HEK-mTLR4 cells were incubated simultaneously with various concentrations of non-biotinylated *E. coli* mpk LPS (LPSEC) or biotinylated *B. vulgatus* mpk LPS (bioLPSBV) for 1 h. Cells were washed and incubated with PE-coupled streptavidin (Strep-PE) for 30 min. PE fluorescence was detected afterwards using flow cytometry.

(c) HEK-mTLR4 cells were incubated with bioLPSBV only according to the experimental setting described in (b). By using different concentrations of bioLPSBV and the resulting detected PE fluorescence, a non-linear regression for a perpendicular hyperbola could be created. The bioLPSBV concentration corresponding to the half-maximal PE intensity equals to KD of bioLPSBV. Squares with error bars represent mean ± SD.

(d) according to (b) 1 x 10^5 HEK-mTLR4 cells were simultaneously incubated with bioLPSBV and LPSEC. For each differentially coloured perpendicular hyperbola binding curve the concentration of biotinylated *B. vulgatus* mpk LPS (bioLPSBV) was varied while the concentration of *E. coli* mpk LPS (LPSEC) was kept constant. According to (b), resulting PE fluorescence was detected by flow cytometry as demonstrated in (a). The detected PE signal is therefore directly proportional to bound bioLPSBV. Each data point represents a distinct combination of LPSEC and bioLPSBV concentrations (n=3). Squares with error bars represent mean ± SD.

(e) Data obtained from (d) were mathematically transformed into a double reciprocal form and plotted into a graph. The sigmoidal binding curves from (d) are therefore transformed into straight lines. The slopes of the straight lines were determined using GraphPad Prism. Squares with error bars represent mean ± SD.

(f) The slopes which were obtained from the double reciprocal plotting in (e) which were derived from the binding curves in (d) were plotted against the corresponding concentration of LPSEC which was kept constant in the experiment. A linearization led to a straight line whose intersection with the x-axis represents the negative value of the dissociation constant ($-K_D$) for the binding of LPS_{EC} to the murine MD-2/TLR4 receptor complex.

Supplemental information 9:

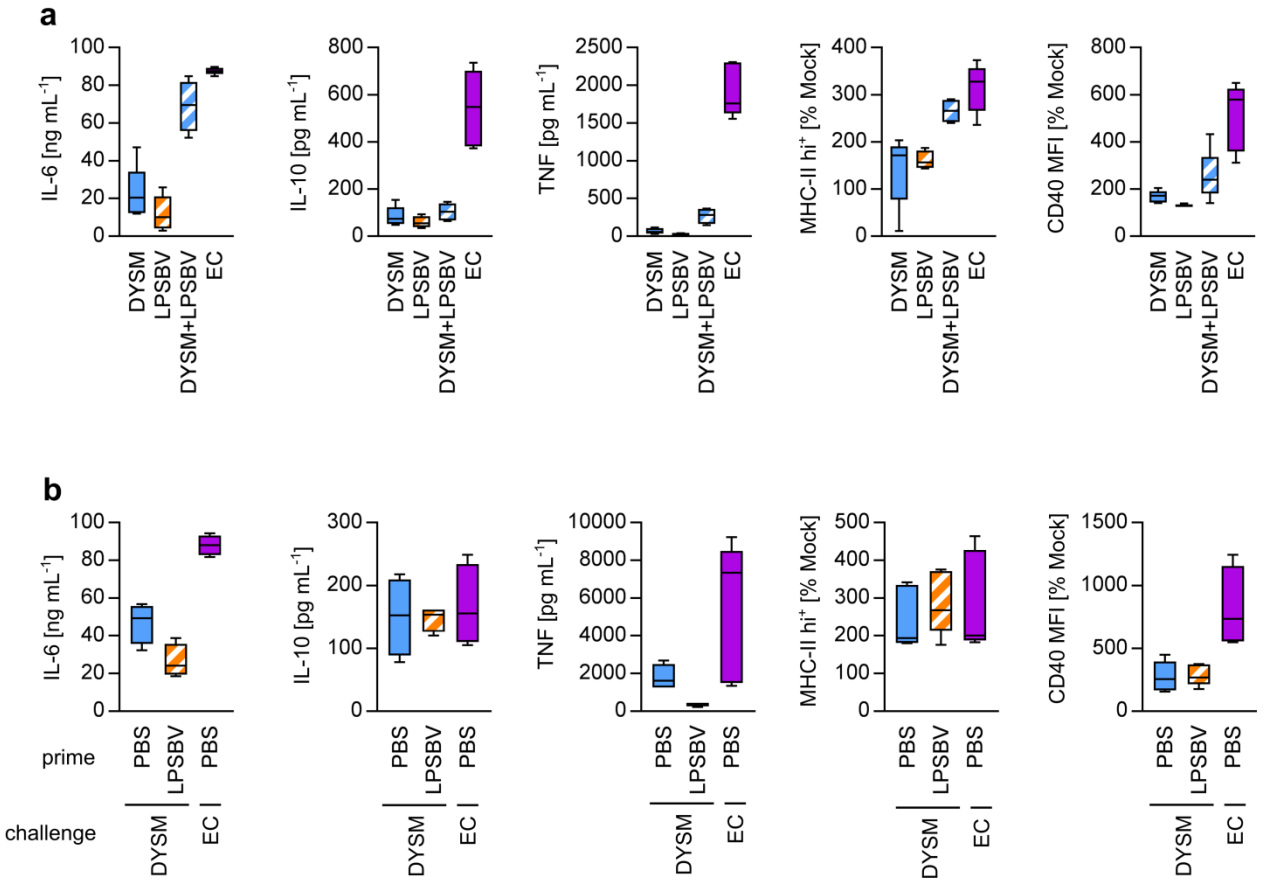

Figure S9:

a) Feces from *Rag1*$^{-/-}$ mice providing intestinal inflammation (DYSM) was autoclaved and prepared as described in Matherials and Methods. Wt BMDCs were stimulated with either DYSM, LPSBV (100 ng mL^{-1}), E. coli mpk (EC, MOI1)) or simultaneous (DYSM + LPSBV). Cytokine secretion was detected by ELISA. Surface expression of MHC-II and CD40 was detected by flow cytometry and normalized to the mock control of BMDCs generated from the same individual. Box plots depict the mean as well as the 25th and 75th percentile, whiskers depict the highest and lowest values.

b) wt BMDCs were stimulated (prime) with either PBS (mock) or LPSBV for 24 h. Medium was changed and cells were stimulated afterwards (challenge) with DYSM or EC (MOI 1). Cytokine secretion was detected by ELISA. Surface expression of MHC-II and CD40 was detected by flow cytometry and normalized to an unchallenged mock control of BMDCs generated from the same individual. Box plots depict the mean as well as the 25th and 75th percentile, whiskers depict the highest and lowest values.

Supplemental References:

1. Ii M, Matsunaga N, Hazeki K, et al. A novel cyclohexene derivative, ethyl (6R)-6-[N-(2-Chloro-4-fluorophenyl)sulfamoyl]cyclohex-1-ene-1-carboxylate (TAK-242), selectively inhibits toll-like receptor 4-mediated cytokine production through suppression of intracellular signaling. Mol Pharmacol 2006;69:1288-95.
2. Matsunaga N, Tsuchimori N, Matsumoto T, et al. TAK-242 (resatorvid), a small-molecule inhibitor of Toll-like receptor (TLR) 4 signaling, binds selectively to TLR4 and interferes with interactions between TLR4 and its adaptor molecules. Mol Pharmacol 2011;79:34-41.
3. Takashima K, Matsunaga N, Yoshimatsu M, et al. Analysis of binding site for the novel small-molecule TLR4 signal transduction inhibitor TAK-242 and its therapeutic effect on mouse sepsis model. Br J Pharmacol 2009;157:1250-62.